Combustion and Flame 161 (2014) 1659–1667

Contents lists available at ScienceDirect

Combustion and Flame

journal homepage: www.elsevier.com/locate/combustflame

Numerical analysis of nanoaluminum combustion in steam

Alexander M. Starik [a,*], Pavel S. Kuleshov [a], Alexander S. Sharipov [a], Nataliya S. Titova [a], Chuen-Jinn Tsai [b]

[a] Central Institute of Aviation Motors, Aviamotornaya St. 2, Moscow 111116, Russia
[b] Institute of Environmental Engineering, National Chiao Tung University, No. 1001, University Road, Hsinchu 30010, Taiwan

ARTICLE INFO

Article history:
Received 19 September 2013
Received in revised form 6 November 2013
Accepted 6 December 2013
Available online 30 December 2013

Keywords:
Kinetic mechanism
Ignition
Combustion
Aluminum–steam system
Nanoparticles
Transport properties

ABSTRACT

The comprehensive analysis of chain mechanism development in the Al–H_2O system is performed on the base of novel reaction mechanism taking into account quantum chemistry studies of potential energy surfaces of the elementary reactions with Al-containing species and estimations of rate constants of corresponding reaction channels. As well the physical properties of Al-containing species involved in the reaction mechanism and needed for the calculation of their transport coefficients are reported. The developed reaction mechanism makes it possible to describe with reasonable accuracy the experimental data on ignition temperature in Al–O_2–Ar and Al–H_2O systems and obtain the qualitative agreement with measured value of laminar flame speed. The two-stage regime of ignition in the Al–H_2O reacting system was revealed both when the aluminum is in the liquid phase and when it comes into steam environment in the gas phase. It was shown that decreasing the ignition temperature one can increase the hydrogen yield in the combustion exhaust.

1. Introduction

Water vapor is a strong oxidizer for several metals. So, the reaction of aluminum with steam yields very high energy density. The other important issue is that the combustion of Al + H_2O mixture produces a significant amount of molecular hydrogen as a combustion product, and reaction of Al with H_2O is considered as a very promising method of hydrogen production [1–3]. Though aluminum is widely utilized as a fuel ingredient in solid propellants and explosives to increase the heat release and, as a result, the specific impulse of rocket engines as well as to reduce the combustion instability [4–6], and a number of researches was addressed the study of kinetics of aluminum combustion (see, for example, [7–11]), the majority of previous works were focused on micron-sized particle burning. The main disadvantage of such particle combustion is that, in this case, large particle can burn only due to diffusion of oxidizer through the metallic oxide shell that forms on the surface of particle, and rate of combustion is limited by the rate of this process [12].

The novel very attractive topic in the combustion of energetic materials is the use of nano-sized Al particles. Such particles exhibit the distinguishing properties compared with micron-sized ones. They feature lower ignition temperature and faster burning rate [8,13–15]. It is believed that such particles undergo fast gasification, and, in this case, atomic aluminum reacts with oxidizer in a gas phase [11]. This supposition has been recently proved by the detection of atomic aluminum during ignition of Al nanoparticles with $d = 80$ nm behind the reflected shock wave [16]. The particles with larger size can be in a liquid phase, and, frequently (see, for example, [17]), the formation of aluminum in gas phase is modeled by simple one step reaction Al(l) ↔ Al(g). In line with the melt-dispersion mechanism [18], at high rate of particle heating, the melting of Al inside the particle is accompanied by volume expansion which creates large pressure in the molten Al. This leads to alumina shell dynamic spallation. As a result, Al liquid core is dispersed into small bare clusters that fly with high velocity. Oxidation of these clusters is not limited by diffusion through the initial alumina shell and occurs in a kinetic mode.

Therefore, it is of great importance to build an adequate gas phase reaction mechanism describing properly the ignition and combustion in the Al–H_2O mixture. It should be emphasized that, in past decade, only a few studies [11,17] were addressed modeling the processes in the Al–H_2O system. However, for the past years, the novel reaction paths in Al–H_2O system were revealed on the base of theoretical calculations [19–21]. This makes it possible to build a more reliable kinetic model for the ignition and combustion of aluminum in steam environment and reconsider the features of chain mechanism development in such a system. The present paper is focused on solving precisely these problems.

2. Kinetic model

The simple estimations show that, for nonoxidized particles with the radius $r < 25$ nm, the time of heating of particle core

* Corresponding author.
E-mail addresses: star@ciam.ru (A.M. Starik), sharipov@ciam.ru (A.S. Sharipov), titova@ciam.ru (N.S. Titova), cjtsai@mail.nctu.edu.tw (C.-J. Tsai).

0010-2180/$ - see front matter © 2013 The Combustion Institute. Published by Elsevier Inc. All rights reserved.
http://dx.doi.org/10.1016/j.combustflame.2013.12.007

caused by energy release in the course of aluminum oxidation and formation of aluminum oxide (Al_2O_3) shell is much higher than the characteristic time of phase transformation. This leads to the rapid destruction of surface layer consisting of Al_2O_3. This conclusion was proved by molecular dynamic calculations [22]. Therefore, the model assumes that nano-sized particles boil or gasify very rapidly and aluminum comes into the environment in the gas or liquid phase. Note that, in accordance with the results of work [18], small liquid Al clusters can form during oxidation even larger sized particles. Certainly, such a model can be applied only to nonoxidized particles.

Nowadays, all developed kinetic mechanisms treated the reaction of atomic aluminum with H_2O molecule as a principal chain initiation reaction. In line with the data reported in [23], both the reaction mechanism of Huang et al. [17] and the mechanism of Washburn et al. [11] considered this reaction path as a complex processes consisting of two channels

$$Al + H_2O = AlOH + H \quad (R1)$$

and

$$Al + H_2O = AlO + H_2, \quad (R2)$$

and the rate constant of R1 channel at high temperature ($T \geqslant 1500$ K) is more than 15 times smaller than that of R2 channel.

However, recent theoretical studies [19,20] revealed that the main reaction path of aluminum with H_2O molecule is the R1 channel, whereas the R2 reaction path is not an elementary one, and rate constant of R1 path is much higher than that of R2 one. Moreover, the reaction mechanisms of Washburn [11] and Huang et al. [17] do not include the important reaction paths with $Al(OH)_2$, $Al(OH)_3$, AlO_2H and other species that were investigated theoretically in recent studies [21,24]. Note that these species were also included in the consideration upon thermodynamic analysis of the composition of combustion exhaust in the premixed Al–H_2–O_2–N_2 flame [25]. In our reaction mechanism we included all these reactions.

In addition, we involved the novel reaction AlO + AlH = AlOH + Al. The rate constant for this reaction was calculated on the base of *ab initio* study of potential energy surface with the use of program package Firefly V. 7.1.G [26]. In accordance with thermochemistry, the activation energy of the reaction AlOH + Al = AlO + AlH must not be lower than 21,200 K. The preliminary quantum-chemical calculations with the use of the unrestricted variant of the second-order Møller–Plesset perturbation theory (UMP2) [26] for solving the Schrödinger equation in relatively large 6-311+G(d,p) basis set revealed that the backward process AlO + AlH → AlOH + Al is nearly barrierless ($E_a \sim 670$ K). The application of more sophisticated quantum-chemical methods that treat electronic correlation more accurately proved this supposition. So, when applying the fourth-order Møller–Plesset perturbation theory in the MP4(SDQ) modification [26] with the same basis set, a slightly lower value of activation energy ($E_a \sim 440$ K) for AlO + AlH = AlOH + Al was obtained. However, when utilizing the coupled-cluster method for solving the Schrödinger equation that proved to be one of the most accurate predictive tools in quantum chemistry, even zero activation barrier value was revealed. So, the calculations using the unrestricted coupled-cluster method including single, double and triple excitations (UCCSD(T)) [26] with 6-311+G(d,p) basis set, suggest that the transition state of this reaction lies more than 4000 K lower than AlO + AlH. Thus, it is worthwhile to include the reaction AlO + AlH = AlOH + Al in the present kinetic model with the rate constant $k(T) = 2.54 \times 10^{13} T^{0.17}$ cm^3 mol^{-1} s^{-1} determined in accordance with methodology used for barrierless reaction [21].

In order to describe the formation of liquid Al_2O_3, in according with [8,17] we treated the reaction of the transformation of gaseous Al_2O_3 to the liquid phase $Al_2O_3(g) \leftrightarrow Al_2O_3(l)$ with the rate constant of 10^{14} s^{-1}. Besides these reaction paths, the developed kinetic model must comprise the submechanism that describes the reactions in the H_2–O_2 system. Earlier, the authors built the kinetic mechanism, which reproduces the large set of experimental data in H_2–O_2–Ar and H_2–air mixtures with rather high accuracy [27,28]. Precisely this reaction mechanism was utilized as a submechanism in the kinetic model for the ignition and combustion in the Al–H_2O system. Thus, the developed reaction mechanism comprises 59 reversible reactions with following species: O, O_2, H, H_2, OH, H_2O, HO_2, H_2O_2, Al, AlO, AlO_2, Al_2O, Al_2O_2, Al_2O_3, $Al_2O_3(l)$, AlH, AlH_2, AlH_3, AlOH, $Al(OH)_2$, $Al(OH)_3$, AlO_2H. Table 1 lists the elementary reactions involved in the model and coefficients needed for the calculations of forward reaction rate constants k_q^+ in line with Arrhenius formula $k_q = A_q T^{n_q} \exp(-E_q/T)$, where A_q is the Arrhenius coefficient, E_q is the activation energy of qth reaction and n_q is the power coefficient. The coefficients for the reactions with Al-containing species presented in Table 1 were chosen on the base of recommendations [8,11,20,21,29]. It should be emphasized that we reconsidered the rate constants for the reactions

$$Al + H + M = AlH + M, \quad (R3)$$

$$AlH + H = Al + H_2 \quad (R4)$$

reported previously by Swihart et al. [29]. The rate constants were estimated on the base of the simplified model of triple collisions for the reaction (R3) and in accordance with methodology used for barrierless reaction for the reaction (R4) [21]. The rate constants of backward reactions k_q^- were calculated with the use of detailed balancing principle. Thermodynamic properties of Al-containing species were taken from the databases reported in [21,30].

It should be emphasized that for some species there are no data on their transport properties. These data are strongly needed to model the deflagrative mode of combustion and the speed of laminar flame propagation. In this work, the coefficients of molecular diffusion, thermal conductivity and viscosity were estimated with the usage of known formulas [31]. The ionization energy E_i, dipole moment μ_i, polarizability α_i and Van-der-Waals collision diameters σ_i, needed for these estimations, were taken from [21,32] or obtained on the base of density functional theory (DFT) calculations at the B3LYP/6-311+G(d,p) level of theory [26]. These parameters as well as the estimated well depth of Lennard-Jones potential for Al-containing species are presented in Table 2.

As in [8,17], we supposed that transport properties of condensed phase of Al and Al_2O_3 are identical to their gas phase counterparts. Though, it should be emphasized that this supposition can be invalid, and the transport properties of rather large clusters $(Al)_n$ and $(Al_2O_3)_n$ with $n > 4$, that form the liquid phase, can differ substantially from those of Al and Al_2O_3 monomers. This issue requires special consideration on the basis of *ab initio* calculations of structure and physical properties of such clusters.

3. Results and discussions

Despite the long history of the studies of aluminum particle burning, the researches of the features of reaction in aluminum–air and aluminum–steam mixtures with the use of detailed gas phase reaction mechanism are fairly limited. These researches allow one to gain an insight both in nano- and in micro-sized aluminum particle combustion. Because the behavior of reaction in Al–air and Al–H_2O mixtures was examined earlier by Huang et al. [8,17], it is reasonable to consider the features of chain mechanism development in such systems, investigated on the base of updated kinetic model, in comparison with that reported in

Table 1
List of reactions and coefficients for calculation of rate constants (cm, mole, s, K).

No.	Reaction	k_q^+			k_q^-			Ref.
		A_q	n_q	E_q	A_q	n_q	E_q	
1.	$H_2O + H = OH + H_2$	8.4E+13	0	10,116	2E+13	0	2600	[27]
2.	$O_2 + H = OH + O$	2.2E+14	0	8455	1.3E+13	0	350	[27]
3.	$H_2 + O = OH + H$	1.8E+10	1	4480	8.3E+9	1	3500	[27]
4.	$O_2 + M = O + O + M$	5.4e18	−1	59,400	6.0e13	0	−900	[27]
5.	$H_2 + M = H + H + M$	2.2E+14	0	48,300	9E+17	−1	0	[27]
6.	$H_2O + M = OH + H + M$	1E+24	−2.2	59,000	2.2E+22	−2	0	[27]
7.	$OH + M = O + H + M$	8.5E+18	−1	50,830	7.1E+18	−1	0	[27]
8.	$H_2O + O = OH + OH$	5.8E+13	0	9059	5.3E+12	0	503	[27]
9.	$H + O_2(+M) = HO_2(+M)$ k_0	3.5e16	−0.41	−565				[27]
	$F_c = 0.5$ k_∞	1.48e12	0.6	0				
10.	$H_2 + O_2 = H + HO_2$	7.39E+5	2.43	26,926				[27]
11.	$H_2O + O = H + HO_2$	4.76E+11	0.372	28,743	1E+13	0	540	[27]
12.	$H_2O + O_2 = OH + HO_2$	1.5E+15	0.5	36,600	3E+14	0	0	[27]
13.	$OH + OH = H + HO_2$	1.2E+13	0	20,200	2.5E+14	0	950	[27]
14.	$OH + O_2 = O + HO_2$	1.3E+13	0	28,200	5E+13	0	500	[27]
15.	$H + H_2O_2 = H_2 + HO_2$	1.7E+12	0	1900	6E+11	0	9300	[27]
16.	$H + H_2O_2 = H_2O + OH$	5E+14	0	5000	2.4E+14	0	40,500	[27]
17.	$HO_2 + HO_2 = H_2O_2 + O_2$	1.8E+13	0	500	3E+13	0	21,600	[27]
18.	$HO_2 + H_2O = H_2O_2 + OH$	1.8E+13	0	15,100	1E+13	0	910	[27]
19.	$OH + HO_2 = H_2O_2 + O$	5.2E+10	0.5	10,600	2E+13	0	2950	[27]
20.	$H_2O_2 + M = OH + OH + M$	1.2E+17	0	22,900	9.1E+14	0	−2650	[27]
21.	$Al + O + M = AlO + M$	3E+17	−1	0				[11]
	$H_2O/2.8/$ $O_2/1.1/$ $H_2/1.1/$							
22.	$Al + O_2 = AlO + O$	2.31E+13	0.17	0				[21]
23.	$AlO + O_2 = AlO_2 + O$	7.12E+12	0.5	13,150				[21]
24.	$AlO_2 = AlO + O$	1E+15	0	44564.6				[11]
25.	$Al_2O = AlO + Al$	1E+15	0	67035.7				[11]
26.	$Al_2O_2 = AlO + AlO$	1E+15	0	59335.7				[11]
27.	$Al_2O_2 = Al + AlO_2$	1E+15	0	74937.1				[11]
28.	$Al_2O_2 = Al_2O + O$	1E+15	0	52,466				[11]
29.	$Al_2O_3 = Al_2O_2 + O$	3E+15	0	49144.4				[11]
30.	$Al_2O_3 = AlO_2 + AlO$	3E+15	0	63915.4				[11]
31.	$Al + H_2O = AlOH + H$ [a]	1.96E+14	−0.09	3744				[20]
		2.78E+06	2.06	438				
32.	$Al + 2H_2O = Al(OH)_2 + H_2$ [b]	1.16E+15	0.5	0				[24], estimated
33.	$Al + 2H_2O = AlOH + H + H_2O$ [b]	1.16E+15	0.5	1260				[24], estimated
34.	$Al + HO_2 = AlO + OH$	1.33E+13	0.17	0				[21]
35.	$Al + HO_2 = AlH + O_2$	1.33E+13	0.17	0				[21]
36.	$AlO + H + M = AlOH + M$	1.99E+15	0.5	0				[21]
37.	$Al + OH + M = AlOH + M$	2.16E+15	0.5	0				[21]
38.	$AlOH + H = AlO + H_2$	2.66E+08	0.82	7844				[20]
39.	$Al + H + M = AlH + M$	9.43E+14	0.5	0				estimated
40.	$AlH_2(+M) = AlH + H(+M)$ k_0	9.68E+14	0	19,962				[29]
	k_∞	1.46E+15	0	23,376				
	$F_c = -4.1 * \exp(-T/21.6) + 5.1 * \exp(-T/493) + \exp(-942/T)$							
41.	$AlH_3(+M) = AlH + H_2(+M)$ k_0	1.01E+15	0	27,089				[29]
	k_∞	1.48E+13	0	30,756				
	$F_c = 0.94 * \exp(-T/885) + 0.06 * \exp(-T/552) + \exp(-3807/T)$							
42.	$AlH + H = Al + H_2$	7.15E+13	0.17	0				estimated
43.	$AlH_2 + H = AlH + H_2$	2E+13	0	0				[29]
44.	$AlH_3 + H = AlH_2 + H_2$	4.75E+09	1.5	0				[29]
45.	$AlOH + O = AlO + OH$	7.53E+12	0.5	4450				[21]
46.	$AlO + OH + M = AlO_2H + M$	2.62E+15	0.5	0				[21]
47.	$AlO + AlH = AlOH + Al$	2.54E+13	0.17	0				estimated
48.	$AlO_2 + H + M = AlO_2H + M$	2.19E+15	0.5	0				[21]
49.	$AlOH + O + M = AlO_2H + M$	2.94E+15	0.5	0				[21]
50.	$AlO + HO_2 = AlOH + O_2$	2.19E+14	−0.08	−35				[21]
51.	$AlOH + HO_2 = AlO_2H + OH$	3.76E+13	0.14	0				[21]
52.	$AlO_2 + H_2O = AlO_2H + OH$	2.63E+02	3.26	3430				[21]
53.	$AlO_2 + H_2 = AlO_2H + H$	4.62E+10	1.39	2940				[21]
54.	$AlO_2 + OH = AlO_2H + O$	2.57E+13	0.17	0				[21]
55.	$AlO_2H + O = AlOH + O_2$	2.14E+13	0.17	0				[21]
56.	$AlO_2H + H = Al(OH)_2$	7.39E+13	0.17	0				[21]
57.	$AlOH + OH = Al(OH)_2$	2.48E+13	0.16	−23				[21]
58.	$Al(OH)_2 + OH = Al(OH)_3$	2.54E+13	0.15	−48				[21]
59.	$Al_2O_3(g) = Al_2O_3(l)$	1E+14	0	0				[8]

[a] The rate constant is the sum of two Arrhenius dependencies.
[b] Reaction products were analyzed in [24], the rate constant was estimated on the base of the simplified model of triple collisions [21].

Table 2
Parameters taken for the calculation of species transport properties used in CHEMKIN Program, as well as ionization energy needed for the calculation of Lennard-Jones potential well depth.

Species	Molecular geometry[a]	Lennard-Jones potential well depth[b], ε/k_B (K)	Lennard-Jones collision diameter[c], σ (Å)	Dipole moment, μ (Debye)	Polarizability, α (Å^3)	Rotational relaxation collision number Z_{rot} at 298 K	Ionization energy, E_i (eV)
Al	0	2836	2.655	0[d]	8.34[d]	1	5.986[d]
AlO	1	1381.2	3.203	4.32[d]	6.7[d]	1	9.46[d]
AlO_2	1	984	3.564	0[c]	9.33[c]	1	9.71[c]
Al_2O	1	2231	3.344	0	12.6	1	8.3
Al_2O_2	2	915.2	4.089	5.9	11.1	1	9.5
Al_2O_3	1	352	4.264	0	9.5	1	10
AlH	1	1101.8	2.975	0.177[d]	6.264[d]	1	8.233[d]
AlH_2	2	526.8	3.184	0.481[d]	5.645[d]	1	7.222[d]
AlH_3	2	119.8	4.001	0[d]	4.39[d]	1	10.793[d]
AlOH	2	668.7	3.374	0.81[c]	6.71[c]	1	9.04[c]
$Al(OH)_2$	2	133.2	4.224	1.32[c]	6.43[c]	1	7.22[c]
$Al(OH)_3$	2	48.5	4.526	0	4.27	1	9.68
AlO_2H	2	216	4.217	5.34[c]	5.19[c]	1	9.8[c]

[a] 0 – atom, 1 – linear molecule, 2 – nonlinear molecule.
[b] Lennard-Jones potential well depth calculated in line with CHEMKIN format.
[c] Data were taken from [21].
[d] Data were taken from NIST Computational Chemistry Comparison and Benchmark Database [32].

[8,17]. All computations were carried out using the CHEMKIN Program package and the PREMIX subroutine [33].

3.1. Ignition in the Al–air mixture

The main supposition of this work model as well as the model of Huang et al. [8] is that the liquid aluminum comes through the spalled alumina shell into environment. Certainly this supposition is needed for some proofs. Following [8] we assumed that liquid aluminum passes into gas phase in the course of reaction

$$\mathrm{Al(l)} = \mathrm{Al(g)}. \qquad \text{(R5)}$$

Huang et al. introduced the rate constant for backward reaction $k_{-R5}(T) = 10^{14}\ \mathrm{s}^{-1}$. The rate constant of forward reaction (R5) was estimated in line with thermochemistry. Following the reference [8] we modeled the ignition process in adiabatic constant-pressure environment. Note that preliminary theoretical calculations exhibited that the rate constant of the reaction Al + N_2 = AlN + N (its energy barrier is approximately equal to 80,000 K or even higher) is much smaller than that for the reaction Al + O_2 = AlO + O and, therefore, it can be assumed that reactions with N_2 molecules do not influence the chain mechanism of aluminum oxidation and nitrogen can be considered as a diluent. Though, it is worth noting that the reactions involving N-containing species (N_2, N, NO, NO_2, N_2O, etc.) should be included in the reaction mechanism in order to describe the formation of aluminum nitrides and NO_x in the combustion exhaust. However, this is out the scopes of the present paper. Figure 1 shows the temporal profiles of species mole fractions and temperature calculated in [8] and computed with the usage of the model of the present work during ignition of a stoichiometric (fuel/air equivalence ratio $\phi = 1$) Al(l)–air mixture at initial temperature $T_0 = 2300$ K and pressure $P_0 = 1$ atm. As in [8], we supposed that aluminum is in a liquid phase. As is seen, the curves predicted by both kinetic models are very close to each other. Some differences are observed for the concentrations of Al, AlO, Al_2O. This appears to be caused by the difference in thermodynamic properties of Al_2O molecule utilized in kinetic model [8] and the model of the present work.

Recently in [16] the experimental data on the ignition of oxidized 80 nm Al particles in Al/O_2/Ar mixture obtained with the shock tube technique were reported. The authors of this work detected the ignition of such particles at $T \geqslant 1200$ K and pressure $P_0 = 7$ atm in the shock tube with working time of 1–2 ms. Shown

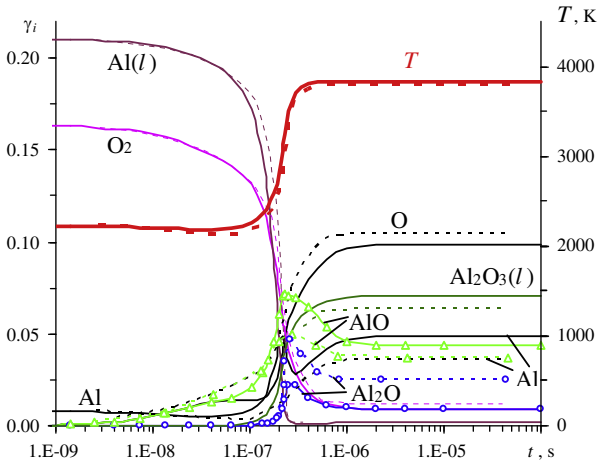

Fig. 1. Evolution of species mole fractions and temperature during ignition in the stoichiometric Al(l)-air mixture calculated in [8] (dotted curves) and computed with the usage of the present work model (solid curves). $T_0 = 2300$ K, $P_0 = 1$ atm.

in Fig. 2 is the variation of temperature vs. time in stoichiometric Al(l)/O_2/Ar mixture at different values of initial temperature computed with the use of the model of this work assuming the aluminum in a liquid phase. One can see that the model predicts the ignition at $t \sim 1$ ms at the temperature $T = 1100$ K that is close to $T_{ign} = 1200$ K reported in [16].

3.2. Flame propagation in the Al–air mixture

Shown in Fig. 3 are the spatial profiles of species mole fractions and temperature in the laminar Al(l)–air stoichiometric ($\phi = 1$) atmospheric pressure flame predicted by both kinetic models considered. And again there exists some discrepancy between the Al, AlO and Al_2O mole fractions calculated with the usage of kinetic model [8] and the model of the present work. However, the values of flame speed U_n predicted by these models are similar. The calculation of Huang et al. [8] gives $U_n = 5.8$ m/s and the model of this work predicts $U_n = 5.6$ m/s. This is not surprised because the Al–O submechanisms involved in the model of the present work and in the model of Huang et al. [8] are very close to each other and provide the identical profiles of atomic oxygen concentration in the flame front. So as the laminar flame speed is determined mainly by the rate of diffusion of the lightest mixture component,

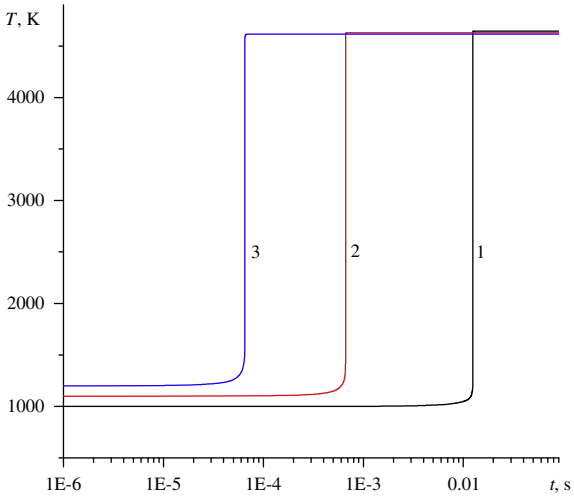

Fig. 2. Temporal profiles of temperature in stoichiometric Al(l)/O_2/Ar mixture (40% O_2/60% Ar) at P_0 = 7 atm and different initial temperatures T_0 = 1000, 1100 and 1200 K (curves 1–3).

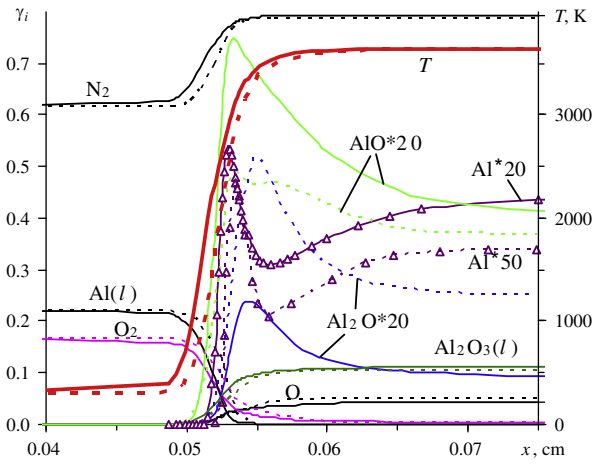

Fig. 3. Variation of species mole fractions and temperature in the stoichiometric Al(l)-air laminar flame calculated in [8] (dotted curves) and computed with the usage of the present work model (solid curves). T_0 = 300 K, P_0 = 1 atm.

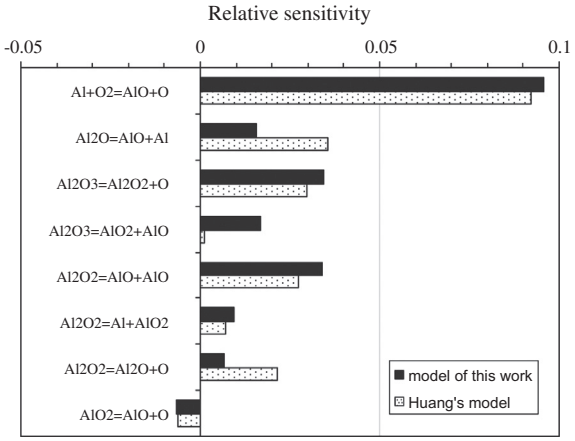

Fig. 4. Sensitivity of laminar flame speed to the reaction rates for the stoichiometric Al(l)-air mixture at T_0 = 300 K, P_0 = 1 atm calculated in [8] and computed with the usage of the model of the present work.

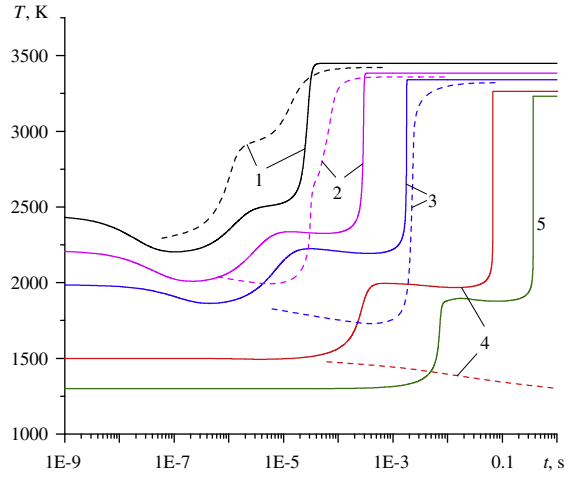

Fig. 5. Evolution of temperature during ignition in the stoichiometric Al(l)-H_2O mixture calculated in [17] (dotted curves) and computed with the usage of the present work model (solid curves) at T_0 = 2800, 2300, 2000, 1500 and 1300 K (curves 1–5), P_0 = 1 atm.

atomic oxygen, from the hot flame region to the cold region, one can expect that the U_n values predicted by these two models should be very close.

The sensitivity analysis demonstrated (see Fig. 4) that, both in the model [8] and in the model of the present work, the U_n value is the most sensitive to the rate constant of the reaction Al + O_2 = AlO + O. The second important reaction in model [8] is Al_2O = AlO + Al, while in the model of the present work, the other two reactions Al_2O_3 = Al_2O_2 + O and Al_2O_2 = 2AlO contribute significantly to the sensitivity of U_n value.

3.3. Ignition in the Al–H_2O system

As was examined above for the aluminum–air mixture, further we will consider the ignition of liquid aluminum in steam environment. Shown in Fig. 5 is the variation of temperature vs. time for the atmospheric stoichiometric (ϕ = 1) Al(l)–H_2O system at different T_0 values calculated with the use of the model of the present work and model [17]. One can see that the predictions of the kinetic models under study differ significantly. So, at high initial temperatures ($T_0 \geqslant 2000$ K), the model [17] predicts shorter ignition delay than that of the model of the present work, and, at smaller temperature, the situation is inverted. Moreover, the model [17] does not provide the ignition at all at T_0 = 1500 K, while the model of the present work predicts the ignition with $\tau_{in} \sim 0.1$ s at T_0 = 1500 K and with $\tau_{in} \sim 0.4$ s at T_0 = 1300 K. In addition, at $T_0 \sim 2000$ K, the behaviors of $\tau_{in}(T_0)$ dependences predicted by two considered models differ principally. The kinetic model [17], after the initial decrease of gas temperature, predicts the continuous growth of T value, while the model of this work gives that after somewhat increase of the temperature, which follows the stage of temperature decrease, the T value falls down slightly again (or does not change at all), and the decrease in the temperature continues up to the ignition event.

When studying numerically the combustion of micrometer-sized aluminum particles with steam, Washburn et al. [11] included detailed chemical reaction mechanism in their model. This mechanism is practically identical to that developed by Huang et al. [17]. The difference between reaction mechanisms [11] and [17] concerns the account for the sensitivity coefficients for some recombination reactions and the reactions of alumina liquid phase formation. Our calculations have shown that these discrepancies do not influence the chain mechanism development and ignition of Al–H_2O mixture.

It should be emphasized that predictions of the model of the present work are in reasonable agreement with the experimental

data on the registration of selfignition temperature for nano-sized Al particles in the Al-water vapor system. So Parr et al. [34] detected the ignition temperature in the range of 1325–1360 K for 24–192 nm Al particles. Low temperature ignition of micron-sized particles in a water vapor medium was also observed by Schoenitz et al. [35]. Our model provides the ignition of aluminum in steam at $T = 1300$ K for atmospheric pressure that is close to the ignition temperature detected in the experiments.

In order to explain a distinction in the predictions of the models under study, let's consider the temporal profiles of species mole fractions during ignition calculated with the use of both considered kinetic mechanisms. Figures 6 and 7 depict such profiles for the atmospheric stoichiometric Al(l)–H_2O mixture at $T_0 = 2300$ and 1500 K, respectively. It follows from the plots shown in Fig. 6 that, at the initial stage of ignition process, the evolution of reagents predicted by two considered models differs considerably. In order to clarify this fact, consider the chain mechanism development providing by both models. The sequence of reaction steps in Al(l) + H_2O reacting system provided by these models is depicted in Fig. 8.

At high initial temperature $T_0 = 2300$ K (Fig. 6), the model [17] predicts identical rates of Al(l) and H_2O concentrations decrease and the rate of H_2 concentration increase at the initial stage. It means that the process Al + H_2O = AlO + H_2 prevails. This reaction is slightly exothermic and results in the temperature increase. As there is no oxidizer for molecular hydrogen in the mixture, its concentration monotonically increases, while the concentration of aluminum oxide AlO diminishes due to recombination processes AlO + Al = Al_2O and 2AlO = Al_2O_2. Atom O, which is needed for Al_2O_3 formation in the reaction Al_2O_2 + O = Al_2O_3, mainly forms due to the dissociation process Al_2O_2 = Al_2O + O.

In the model of the present work, the occurrence of another chain-initiation reaction Al + H_2O = AlOH + H (it is also exothermic) immediately results in the formation of active H atoms, which in the course of two successive processes H + H_2O = H_2 + OH and H + OH = H_2 + O give OH radical and O atom. On the one hand, the recombination of AlOH with OH leads to the formation of $Al(OH)_2$ and $Al(OH)_3$ as well as AlO_2H in the reaction $Al(OH)_2$ = AlO_2H + H. These species are long-lived and delay the ignition. On the other hand, O atoms react with AlOH and H_2 generating AlO (and, as consequence, Al_2O_2 and Al_2O_3) and H_2O. As well, AlO forms in the course of reaction AlOH + Al = AlO + AlH. This reaction decreases the rate of AlOH, $Al(OH)_2$, $Al(OH)_3$ and AlO_2H production. From the plots shown in Figs. 6 and 7 one can see that, after the rapid decrease, the concentration of water vapor begins to increase up to the ignition time instant, and this promotes the ignition. These two contradicted factors result in longer delay time at high

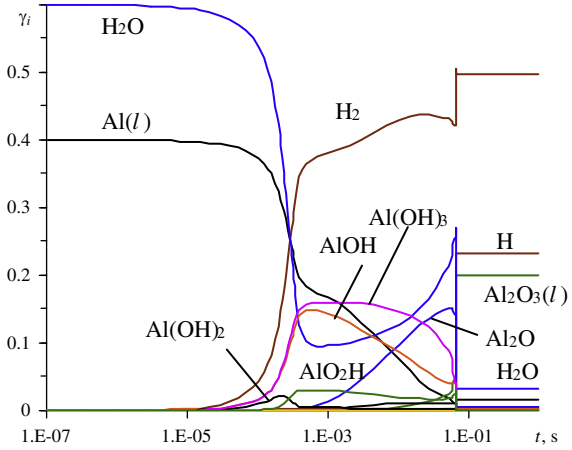

Fig. 7. Variation of species mole fractions during the ignition of stoichiometric Al(l)-H_2O mixture computed with the usage of the present work model at $T_0 = 1500$ K, $P_0 = 1$ atm.

temperatures and, on the contrary, in shorter one at low temperatures in the predictions of our model compared to those of the model [17]. It should be noted that at $T_0 \leqslant 1500$ K (see Fig. 5) the model [17] does not predict the ignition at all and, hence, cannot describe the experimental data on the ignition temperature [34].

Computations showed that the smaller the initial temperature is, the higher is the yield of molecular hydrogen in the combustion products. Thereby, in order to produce more hydrogen during combustion of nanoaluminum in water vapor, it is necessary to use small nanoparticles that allow one to decrease the ignition temperature. The difference in the H_2 yield in the cases with $T_0 = 1300$ and 2300 K achieves 25%.

Let us consider now how ignition temperature and induction time change when aluminum in the gas phase reacts with steam. Remind that such regime of combustion can be realized for small nonoxidized nano-sized particles [22]. Figure 9 shows the temporal profiles of gas temperature for the stoichiometric Al(g)–H_2O mixture at different initial temperatures, predicted by the model [17] and the model of the present work. One can see that, in this case, the ignition temperature and induction time are smaller than those for the liquid aluminum combustion, and both models under study provides this tendency. These results are qualitatively consistent with the experimental data (see [8]) that demonstrates the decrease in ignition temperature with decreasing particle diameter. As it follows from the plots shown in Fig. 9, both models predict that the stoichiometric Al(g)–H_2O mixture ignites at

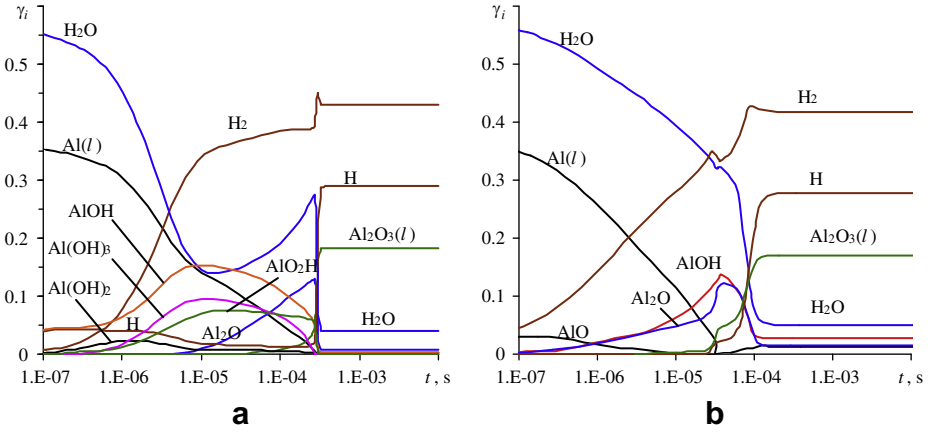

Fig. 6. Variation of species mole fractions during the ignition of the stoichiometric Al(l)-H_2O mixture computed with the usage of the present work model (a) and calculated in [17] (b) at $T_0 = 2300$ K, $P_0 = 1$ atm.

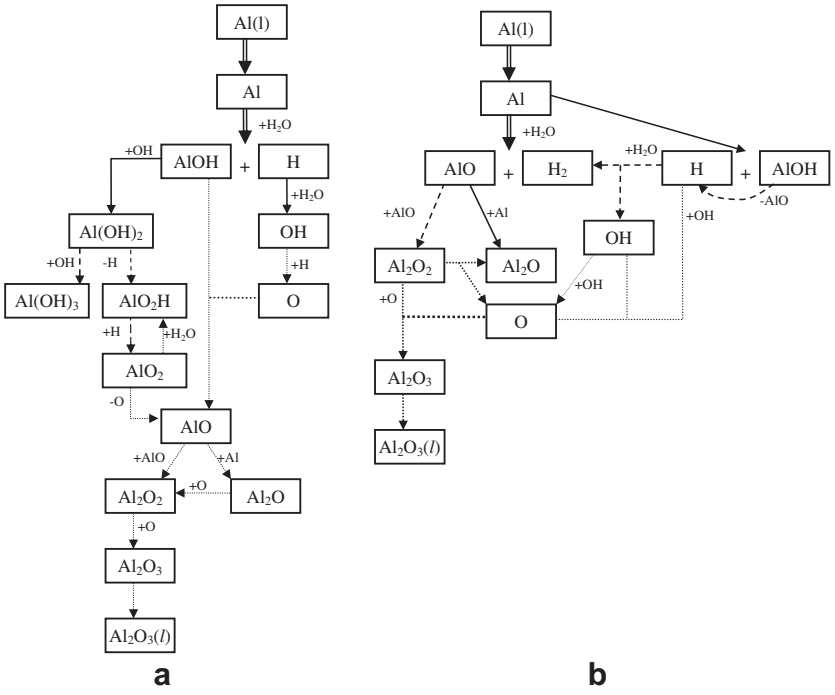

Fig. 8. The schemes of chain-mechanism development in the Al(*l*)-H_2O reacting system in accordance with our model (a) and the model [17] (b). Dotted, dashed and solid arrows denote the reaction channels with different rates (in ascending order).

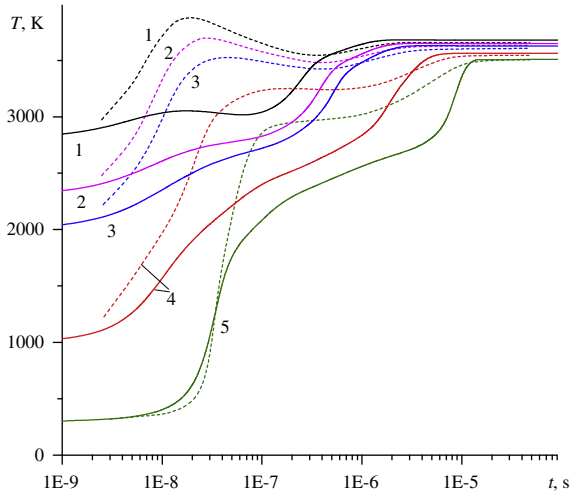

Fig. 9. Evolution of temperature during ignition in the stoichiometric Al(g)-H_2O mixture calculated in [17] (dotted curves) and predicted by the model of the present work (solid curves) at T_0 = 2800, 2300, 2000, 1000 and 300 K (curves 1–5), P_0 = 1 atm.

T_0 = 300 K. However the temperature profiles calculated with the use of model [17] and the model of the present work differ notably. The model [17] predicts the existence of maximum in the temperature behavior at $T_0 \geqslant 2000$ K, while the model of the present work does not give such a type of temperature profile.

Figure 10 depicts the time history of species mole fractions calculated with the use of both models under study for the stoichiometric Al(g)–H_2O mixture at T_0 = 2300 K and P_0 = 1 atm. One can see that the model [17] gives the appearance of AlO and H_2 at the first stage due to the reaction of Al with H_2O. Because this reaction is slightly exothermic, the temperature, at the initial stage, increases. Further, in line with model [17], AlO reacts with aluminum atom AlO + Al = Al_2O. As a result, the concentration of Al_2O rises drastically and becomes greater than that of AlO. This reaction occurs with high energy release ($\Delta H \sim 560$ kJ/mol). That is why the model [17] provides a strong increase in the temperature up to the time instant $t \sim 2 \cdot 10^{-8}$ s. At this time instant the concentration of H_2 achieves its local maximum and then varies only slightly due to competition of the process of H_2 formation in the course of reaction Al + H_2O = AlO + H_2 and the process of H_2 elimination owing to its dissociation H_2 + M = H + H + M. Because the dissociation process is endothermic, the temperature, at first stage, decreases and, then, starts to increase due to formation of condensed phase of Al_2O_3.

The model of the present work predicts the fast arise of AlOH and atomic hydrogen at initial stage. The absence of AlO does not lead to the fast formation of Al_2O and, consequently, to the great energy release. The temperature rises monotonically mostly due to heat release in the course of reaction AlO_2 + H + M = AlO_2H + M, and then, at the final stage, owing to formation of Al_2O_3 in the liquid phase. Thus, one can conclude that when aluminum both in the liquid and in the gas phases reacts with the water vapor, there exists two-stage regime of ignition. The final temperature in the combustion exhaust is higher when we deal with the combustion of small sized particles which can gasify very rapidly and, as a result, gaseous aluminum reacts with steam.

3.4. Flame propagation in the Al–H_2O mixture

Because the equilibrium temperature achieved during combustion of Al–air system is notably higher than that for the Al–H_2O mixture, the flame speed in the former case must be greater than that in the latter one. This conclusion was proved by calculations of Huang et al. [17]. Our computations, based on the reaction mechanism of the present work, exhibit the similar results. However, the reaction mechanism of the present work provides higher values of the speed of laminar flame propagation U_n than the Huang et al. mechanism [17], while the values of final flame temperature are identical to those predicted by Huang et al. [17]. Depicted in Fig. 11 is a comparison of U_n and T_e predicted by the mechanisms of [17] and the present work for Al(*l*)–H_2O system at various ϕ values. As is seen, the difference in the flame speed calculated with the

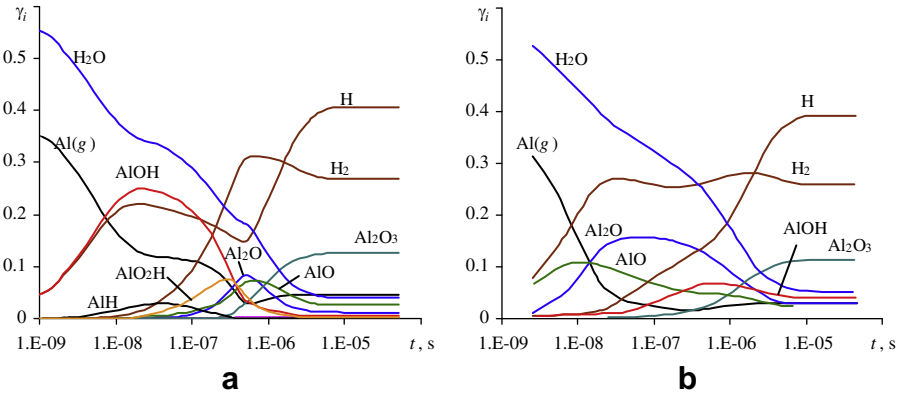

Fig. 10. Variation of species mole fractions during the ignition of the stoichiometric Al(g)-H_2O mixture calculated by using the model of the present work (a) and calculated in [17] (b) at T_0 = 2300 K, P_0 = 1 atm.

use of reaction mechanisms under consideration can achieve a factor of 1.6. The maximal value of U_n predicted by the model of this work is achieved at ϕ = 0.9 (T_0 = 800 K, P_0 = 1 atm) and equals to 1.66 m/s. The sensitivity analysis showed that U_n value is the most sensitive to the rate constants of the reactions AlH + H = Al + H, Al + H + M = AlH + M and Al + H_2O = AlOH + H (see Fig. 12). It should be emphasized that precisely rate coefficients of these reactions were reconsidered compared to the model [17]. Moreover, the Al + H_2O reaction channel, included in the Huang et al. reaction mechanism [17], differs principally from that involved in the model of the present work. This leads to substantial distinction in the variation of species concentrations of mixture components and, especially, the concentration of H atoms in the flame front predicted by the model of Huang et al. [17] and the model of the present work. Because the laminar flame speed for the Al–H_2O reactive system is determined mainly by the rate of the diffusion of H atoms, the U_n values predicted by these two models must be different. At the same time, the value of final temperature in the combustion products is determined by the thermodynamic properties of individual species taken in the kinetic model. These properties do not differ significantly for both models under study. That is why the T_e values predicted by the models of [17] and the present work for Al(l)–H_2O system are practically identical despite the substantial difference in the reaction mechanisms.

The variation of species mole fractions and temperature in the flame front region for the Al(l)–H_2O system with ϕ = 0.9 predicted

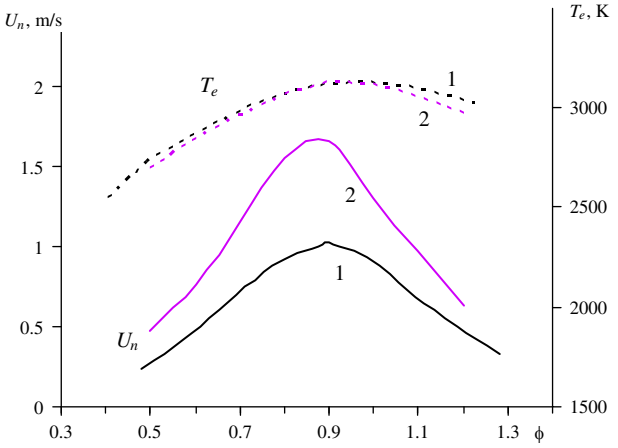

Fig. 11. Flame speed U_n and final flame temperature T_e values (solid and dotted lines) vs. fuel/oxidizer equivalence ratio ϕ of the Al(l)-H_2O mixture calculated in [17] and predicted by the model of the present work (curves 1 and 2, respectively) at T_0 = 800 K and P_0 = 1 atm.

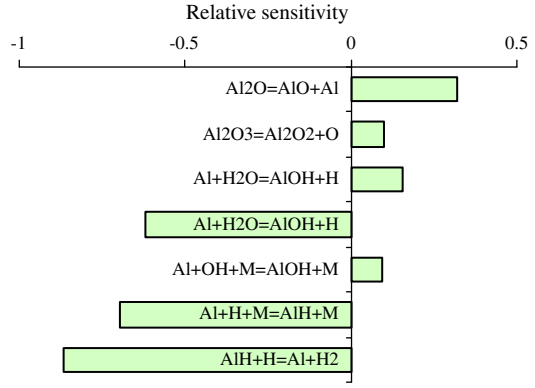

Fig. 12. Sensitivity of laminar flame speed to the reaction rates for the stoichiometric Al(l)-H_2O mixture at T_0 = 800 K, P_0 = 1 atm calculated with the usage of the model of the present work.

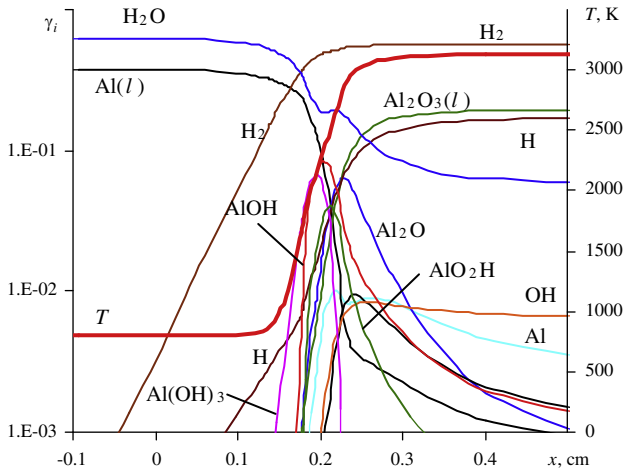

Fig. 13. Variation of species mole fractions and temperature in the Al(l)-H_2O laminar flame predicted by the model of the present work at T_0 = 800 K, P_0 = 1 atm, ϕ = 0.9.

by the model of the present work is depicted in Fig. 13. One can see that the main combustion products are H_2 and liquid Al_2O_3, and the final temperature does not exceed 3250 K. The mole fraction of molecular hydrogen γ_{H_2} in the combustion products, at such conditions, is as large as 0.55. The content of Al_2O_3 in the liquid phase is much smaller ($\gamma_{Al_2O_3}$ = 0.2). The third component with

notable mole fraction is atomic hydrogen ($\gamma_H = 0.15$). The concentrations of other mixture components are much smaller.

Unfortunately, until now there have been no experimental data on the flame speed in the Al–H_2O system with dust particles of different sizes. Only the U_n value for the system of aluminum particles being in the liquid water were measured [13]. Nevertheless, it is interesting to compare the measurements [13] with the predictions of the model of this work. Certainly, the comparison can be considered as qualitative only. In the experiments [13], the oxidized Al nanoparticles with diameter of 38 nm were used, and the concentration of Al_2O_3 in the whole particle volume was equal to 54.3 wt%. The system was primarily ignited and the change in the position of flame front was detected.

We assumed that burning of Al nanoparticles occurs in steam environment after vaporization of liquid water and took into consideration that Al and Al_2O_3 in a particle can be both in solid and in liquid phases. Therefore, we considered the combustion of the mixture with following composition Al(s,*l*)/Al_2O_3(s,*l*)/H_2O(g) = 1/0.2228/1.5. In addition, we supposed that particles burn in water vapor, if they are in a liquid phase. So far as, in line with the theory reported in [36], the melting temperature for Al particles with $d = 38$ nm is approximately equal to 840 K [8]. The thermodynamic properties for combined solid-liquid phase Al(s,*l*) and Al_2O_3(s,*l*) were taken from Janaf tables [37]. In this case, the reactions Al(*l*) = Al(g) and Al_2O_3(*l*) = Al_2O_3(g) were replaced as Al(s,*l*) = Al(g) and Al_2O_3(s,*l*) = Al_2O_3(g). In experiments [13] at $P_0 = 100$ atm the flame speed was detected in the range of 5.5–8.5 m/s. Our model predicts $U_n = 8.9$ m/s, that is in reasonable coincidence with experimental data, though, in this case, we can say only about qualitative agreement, because the experimental conditions cannot be modeled exactly.

4. Conclusions

The extended reaction mechanism for the Al–H_2O system combustion treated the recent *ab initio* and theoretical studies of the elementary reactions in such system was built. In contrast, previous kinetic models of Huang et al. [17] and Washburn et al. [11], this mechanism suggests the novel channel of chain initiation Al + H_2O = AlOH + H and involves the reactions with additional species $Al(OH)_2$, $Al(OH)_3$ and AlO_2H. The developed reaction mechanism allows one to describe with reasonable accuracy the experimental data on ignition temperature obtained for combustion of nanoaluminum in oxygen and in water vapor.

The computations showed that in the Al–H_2O mixture when aluminum is both in the liquid and in the gas phase, there exists two-stage regime of ignition and this fact is determined by the features of chain mechanism development. If the aluminum comes into the steam environment in a liquid phase, the ignition occurs at higher temperature ($T_{ign} = 1300$ K for stoichiometric atmospheric Al–H_2O mixture) than that when Al reacts with water vapor in the gas phase. The decrease in the initial temperature leads to the increase in the yield of molecular hydrogen in combustion exhaust. In the laminar atmospheric flame in Al(*l*)–H_2O mixture close to stoichiometric one, the mole fraction of H_2 can be as large as 0.55, while the mole fractions of the other major components, liquid Al_2O_3 and atomic hydrogen, are equal to 0.2 and 0.15 respectively. Because the aluminum in the gas phase reacts with steam much faster even at low temperatures, it is reasonable in the process of hydrogen production to use small nano-sized non-oxidized Al particles that, due to their rapid gasification, can provide the burning of aluminum in the gas phase.

Acknowledgments

This work was supported by the Russian Foundation for Basic Research (Grants 12-08-92008 and 11-01-00920).

References

[1] E. Shafirovich, V. Diakov, A. Varma, Combust. Flame 144 (1–2) (2006) 415–418.
[2] M.S. Vlaskin, E.I. Shkolnikov, A.V. Lisicyn, A.V. Bersh, A.Z. Zhuk, Int. J. Hydrogen Energy 35 (5) (2010) 1888–1894.
[3] F. Franzoni, M. Milani, L. Montorsi, V. Golovitchev, Int. J. Hydrogen Energy 35 (4) (2010) 1548–1559.
[4] V. Yang, T.B. Brill, W.Z. Ren (Eds.), Solid propellant chemistry, combustion, and motor interior ballistics, in: AIAA Progress in Aeronautics and Astronautics, 2000, p. 663.
[5] A. Dokhan, E.W. Price, J.M. Seitzman, R.K. Sigman, Proc. Combust. Inst. 29 (2) (2002) 2939–2945.
[6] A. Ingenito, C. Bruno, J. Propul. Power 20 (6) (2004) 1056–1064.
[7] J. Servaites, H. Krier, J.C. Melcher, R.L. Burton, Combust. Flame 125 (1–2) (2001) 1040–1054.
[8] Y. Huang, G.A. Risha, V. Yang, R.A. Yetter, Combust. Flame 156 (1) (2009) 5–13.
[9] M.T. Swihart, L. Catoire, J. Phys. Chem. A 105 (1) (2001) 264–273.
[10] M.W. Beckstead, Y. Liang, K.V. Pudduppakkam, Combust. Explos. Shock Waves 41 (6) (2005) 622–638.
[11] E.B. Washburn, J.N. Trivedi, L. Catoire, M.W. Beckstead, Combust. Sci. Technol. 180 (8) (2008) 1502–1517.
[12] R.A. Yetter, F.L. Dryer, Metal Particle Combustion and Classification, Micro-Gravity Combustion: Fire in Free Fall, Academic Press, 2001. p. 419.
[13] G.A. Risha, J.L. Sabourin, V. Yang, R.A. Yetter, S.F. Son, B.C. Tappan, Combust. Sci. Technol. 180 (12) (2008) 2127–2142.
[14] P. Escot Bocanegra, V. Sarou-Kanian, D. Davidenko, C. Chauveau, I. Gökalp, Prog. Propul. Phys. 1 (2009) 47–62.
[15] N. Moallemi, M. Bidbadi, M. Jadidi, M.E. Hosseini, Aust. J. Basic Appl. Sci. 5 (12) (2011) 1991–1998.
[16] P. Lynch, G. Fiore, H. Krier, N. Glumac, Combust. Sci. Technol. 182 (7) (2010) 842–857.
[17] Y. Huang, G.A. Risha, V. Yang, R.A. Yetter, Analysis of nano-aluminum particle dust cloud combustion in different oxidizer environments, in: 43rd AIAA Aerospace Sciences Meeting and Exhibit 10–13 January 2005, Reno, Nevada. AIAA 2005-738.
[18] V.I. Levitas, Combust. Flame 156 (2) (2009) 543–546.
[19] S. Álvarez-Barcia, J.R. Flores, Chem. Phys. 382 (1–3) (2011) 92–97.
[20] A. Sharipov, N. Titova, A. Starik, J. Phys. Chem. A 115 (17) (2011) 4476–4481.
[21] A.S. Sharipov, N.S. Titova, A.M. Starik, Combust. Theory Model. 16 (5) (2012) 842–868.
[22] T.J. Campbell, G. Aral, S. Ogata, R.K. Kalia, A. Nakano, P. Vashishta, Phys. Rev. B 71 (20) (2005) 205413.
[23] R.E. McClean, H.H. Nelson, M.L. Campbell, J. Phys. Chem. 97 (38) (1993) 9673–9676.
[24] S. Álvarez-Barcia, J.R. Flores, Chem. Phys. 374 (1–3) (2010) 131–137.
[25] J. Guo, J.M. Goodings, A.N. Hayhurst, Combust. Flame 150 (1–2) (2007) 127–136.
[26] A.A. Granovsky, Firefly. <http://classic.chem.msu.su/gran/firefly/index.html>; version 7.1.G.
[27] A.M. Starik, N.S. Titova, A.S. Sharipov, V.E. Kozlov, Combust. Explos. Shock Waves 46 (5) (2010) 491–506.
[28] A.M. Starik, N.S. Titova, A.S. Sharipov, Kinetic mechanism of H_2–O_2 ignition promoted by singlet oxygen $O_2(a^1\Delta_g)$, in: G.D. Roy, S.M. Frolov (Eds.), Deflagrative and Detonative Combustion, Torus Press, Moscow, 2010, pp. 19–42.
[29] M.T. Swihart, L. Catoire, B. Legrand, I. Gökalp, C. Paillard, Combust. Flame 132 (1–2) (2003) 91–101.
[30] E. Goos, A. Burcat, B. Ruscic, Ideal gas thermochemical database with updates from active thermochemical tables. <ftp://ftp.technion.ac.il/pub/supported/aetdd/thermodynamics>.
[31] J.O. Hirschfelder, C.F. Curtiss, R.B. Bird, Molecular Theory of Gases and Liquids, Wiley, N.Y., 1954.
[32] R.D. Johnson III, NIST Computational Chemistry Comparison and Benchmark Database, NIST Standard Reference Database, Number 101, Release 15b, August 2011. <http://cccbdb.nist.gov>.
[33] R.J. Kee, F.M. Rupley, J.A. Miller, M.E. Coltrin, J.F. Grcar, E. Meeks, et al. CHEMKIN Release 4.0, Reaction Design Inc., San Diego, CA. 2004.
[34] T.P. Parr, C. Johnson, D. Hanson-Parr, K. Higa, K. Wilson, Evaluation of advanced fuels for underwater propulsion, in: 39th JANNAF Combustion Subcommittee Meeting, December 2003.
[35] M. Schoenitz, C.-M. Chen, E.L. Dreizin, J. Phys. Chem. B 113 (15) (2009) 5136–5140.
[36] C.R.M. Wronski, Br. J. Appl. Phys. 18 (12) (1967) 1731–1737.
[37] M.W. Chase Jr., C.A. Davies, J.R. Downey, D.J. Frurip Jr., R.A. McDonald, A.N. Syverud, NIST JANAF THERMOCHEMICAL TABLES, 1985, Version 1.0. <http://kinetics.nist.gov/janaf/>